

Water Body Temperature Model for Assessing Climate Change Impacts on Thermal Cooling

Ken Strzepek, Charles Fant, Yohannes Gebretsadik, Megan Lickley, Brent Boehlert, Steven Chapra, Eric Adams, Andrzej Strzepek and C. Adam Schlosser



Report No. 280
May 2015

The MIT Joint Program on the Science and Policy of Global Change combines cutting-edge scientific research with independent policy analysis to provide a solid foundation for the public and private decisions needed to mitigate and adapt to unavoidable global environmental changes. Being data-driven, the Program uses extensive Earth system and economic data and models to produce quantitative analysis and predictions of the risks of climate change and the challenges of limiting human influence on the environment—essential knowledge for the international dialogue toward a global response to climate change.

To this end, the Program brings together an interdisciplinary group from two established MIT research centers: the Center for Global Change Science (CGCS) and the Center for Energy and Environmental Policy Research (CEEPR). These two centers—along with collaborators from the Marine Biology Laboratory (MBL) at Woods Hole and short- and long-term visitors—provide the united vision needed to solve global challenges.

At the heart of much of the Program's work lies MIT's Integrated Global System Model. Through this integrated model, the Program seeks to: discover new interactions among natural and human climate system components; objectively assess uncertainty in economic and climate projections; critically and quantitatively analyze environmental management and policy proposals; understand complex connections among the many forces that will shape our future; and improve methods to model, monitor and verify greenhouse gas emissions and climatic impacts.

This reprint is one of a series intended to communicate research results and improve public understanding of global environment and energy challenges, thereby contributing to informed debate about climate change and the economic and social implications of policy alternatives.

Ronald G. Prinn and John M. Reilly,
Program Co-Directors

For more information, contact the Program office:

MIT Joint Program on the Science and Policy of Global Change

Postal Address:

Massachusetts Institute of Technology
77 Massachusetts Avenue, E19-411
Cambridge, MA 02139 (USA)

Location:

Building E19, Room 411
400 Main Street, Cambridge

Access:

Tel: (617) 253-7492

Fax: (617) 253-9845

Email: globalchange@mit.edu

Website: <http://globalchange.mit.edu/>

Water Body Temperature Model for Assessing Climate Change Impacts on Thermal Cooling

Ken Strzepek^{*†}, Charles Fant^{*}, Yohannes Gebretsadik[‡], Megan Lickley^{*}, Brent Boehlert[§], Steven Chapra^{**}, Eric Adams^{*}, Andrzej Strzepek^{*} and C. Adam Schlosser^{*}

Abstract

We develop and test a physically based semi-Lagrangian water body temperature model to apply climatological data and thermal pollution from river-based power plants to historical river flow data in order to better understand climate change impacts on surface water temperature and thermal power plant withdrawal allowances. The model is built for rapid assessment and use in Integrated Assessment Models. We first test the standalone model on a 190km river reach, the Delaware River, where we have detailed flow and temperature data. An R^2 of 0.88 is obtained on hourly data for this initial test. Next, we integrate the standalone temperature model into a series of models—rainfall-runoff model, water demand model, water resource management model, and power plant uptake and release model—for the contiguous USA (CONUS), with about 19,000 segments total. With this system in place, we then validate the standalone water temperature model within the system for 16 river stations throughout the CONUS, where we have measured daily temperature data. The model performs reasonably well with a median R^2 of 0.88. A variety of climate and emissions scenarios are then applied to the model to test regions of higher vulnerability to river temperature environmental violations, making use of output from two GCMs and six emissions scenarios focusing on projections out to 2050. We find that the two GCMs project significantly different impacts to water temperature, driven largely by the resulting changes in streamflow from the two models. We also find significantly different impacts on the withdrawal allowed by thermal power plants due to environmental regulations. Potential impacts on generation are between +3% and -4% by 2050 for the unconstrained emissions case and +3.5% to -2% for the stringent GHG mitigation policy (where 1% is equivalent to 32 TWh, or about 3 billion USD/year using 2005 electricity prices). We also find that once-through cooling plants are most vulnerable to climate change impacts, with summer impacts ranging from -0.8% to -6% for the unconstrained emissions case and +2.1% to -3.7% for the stringent GHG emissions case.

Contents

1. INTRODUCTION	2
2. DATA AND METHODS	3
2.1 Climate Scenarios.....	4
2.2 Runoff Model	6
2.2.1 Water Demands.....	6
2.3 Water Resources Management Model	7
2.4 Model of Water-body Temperature.....	8
2.4.1 River Network	8
2.4.2 River Geometry	8
2.4.3 Heat Budget Model	9

* Joint Program on the Science and Policy of Global Change, Massachusetts Institute of Technology, MA, USA.

† Corresponding author (Email: strzepek@mit.edu).

‡ UNU - World Institute for Development Economics Research, Helsinki, Finland.

§ Industrial Economics, Inc., Cambridge, MA, USA.

** Tufts University, Medford, MA, USA.

2.5 Power Plant Model	11
3. MODEL VALIDATION	13
3.1 The Delaware River	14
3.2 Multi-HUC Model Testing.....	16
4. RESULTS.....	17
4.1 Baseline	17
4.2 Future Changes.....	19
4.3 Valuation of Mitigation Benefits.....	23
5. CONCLUSION	25
6. REFERENCES	26

1. INTRODUCTION

River temperatures are critical for maintaining both the integrity of the aquatic ecosystem, and the cooling capacity for thermoelectric power production. Temperature is often referred to as the most critical water parameter as it influences the growth, reproductivity and metabolism of fish, the ecosystem composition and productivity, the level of oxygen and carbon dioxide uptake, and the rate of chemical reactions (Brungs *et al.*, 1977; MacLeod and Pessah, 1973; Graham, 1949). Temperature is also an important parameter for the production of energy in the United States, as power plants require cold water for cooling purposes and efficient production of energy. Presently, 91% of energy production in the United States comes from thermoelectric power plants (nuclear, coal, natural gas, petroleum) (EIA, 2013) and accounts for just over 40% of total freshwater withdrawals (Kenny *et al.*, 2014). Since many of the withdrawals are used for cooling purposes, the effluent water from power plants is much warmer than the natural river temperature.

Due to the harmful impacts that warm river temperatures can have on fish, water temperature has been regulated under the Federal Water Pollution Control Act (a.k.a. the Clean Water Act) in Sections 316a and 316b. Though restrictions change from state to state, generally river temperatures are restricted to a 2.8°C temperature increase from a pollution source (once fully mixed), with a fully mixed temperature not exceeding upper limits ranging between 23°C and 29°C, location dependent. Until recently, power plants have adapted to meet these restrictions with technological improvements such as cooling towers or cooling ponds. However, in 2012, despite these improvements, power production suffered due to increased drought and heat waves. The Millstone nuclear power plant, for example, was forced to shut down due to water in Long Island Sound being too warm to cool the plant. In Illinois that year, cooling ponds were exceeding 37°C and the EPA granted special permission for plant operations despite exceeding temperature restrictions and water withdrawal limitations. As climate change worsens over the coming decades, we can expect a higher frequency of these events. The IPCC (2014) reports that we should expect warmer air temperatures, prolonged droughts, and decreased snow packs and flows, all of which would negatively impact the availability of cold freshwater. The extent of these impacts on power production, however, remains unclear.

There are many studies that provide some useful insight into the impacts of climate on river temperature and/or power production. Earlier research provides simple relationships between air temperature, elevation and the resulting river temperature (Stefan and Preud'homme, 1993;

Walker and Lawson, 1993). While these methods are still useful in their simplicity, more complete and dynamic models have since been developed. Among these models there is a broad range of spatial and temporal resolution as well as complexity in terms of hydrological and atmospheric interactions with water temperature. There are now multiple global, large basin routing models (van Vliet *et al.*, 2012a; Olivera *et al.*, 2000; Ngo-Duc *et al.*, 2007) which use variable velocity to model river runoff in the worlds 20 largest rivers. There are more highly resolved and physically complex models like Gooseff *et al.* (2005), which looks at climate change impacts on a river downstream of a small reservoir and accounts for kinematic wave flow routing, atmosphere and stream-bed heat exchange fluxes. This allows for a more in-depth analysis at a single location. Herb and Stefan (2010) includes wetlands and groundwater along with atmospheric heat transfer, and Yearsley (2012) uses a grid-based approach and includes propagation of uncertainty to model climate impacts on stream temperature.

With the exception of van Vliet *et al.* (2012b), much of the literature on climate impacts on power systems is limited to individual plant analysis. Förster and Lilliestam (2010) model the range of thermo power production constraints under changes in stream temperature and flow. Chandel *et al.* (2011) model the impacts of climate policy and a CO₂ price on freshwater use in thermoelectric power production. The networked aspect of river modeling is especially important for modeling thermal pollution as it is cumulative, i.e. upstream plants can impact downstream withdrawal temperatures. The methods used in van Vliet *et al.* (2012b), however, account for climate impacts on a networked river model in order to assess broad scale energy production vulnerability in Europe and the U.S. They incorporate an electricity production model to account for thermal pollution and loss of electricity production as a result of climate change. They also use a temperature change across the heat exchanger of 3°C, which is low—typical temperature changes are closer to 11–12°C (Adams and Harleman, 1979).

In this paper, we present a physically based networked semi-Lagrangian river temperature transport model for the United States that runs hourly at an 8-digit HUC scale and includes thermal discharge from energy sources. Our standalone water temperature model follows many other methods such as Yearsley (2009), and we've adapted this method to look at specific water and energy systems. The model is intended to fit efficiently into an integrated assessment model framework for climate change impact studies. Consequently, we integrate our water temperature model into a series of models to quantify the climate change impact on power plant withdrawal and release, enforcing conservative environmental regulations. These data and methods are described in Section 2. In Section 3, the model validation is presented. In Section 4, we present the results of the climate change impact analysis. Finally, in Section 5, the main conclusions of the study are discussed.

2. DATA AND METHODS

In this section, we describe the full suite of models used in this analysis (summarized in **Figure 1**). First, a series of climate and emissions scenarios are developed to understand the impacts of mitigation, climate sensitivity, and GCM model structure. Second, a rainfall-runoff

model is employed to estimate the impacts of changes in climate to changes in surface water supply. Third, we develop estimates of changes in water demands, which respond to changes in population and climate. Fourth, these data are integrated into a water resource management model that systematically simulates surface-water allocation as well as reservoir storage and release. Fifth, these managed flows and reservoir volumes are input into the water temperature model. Finally, a physically based rule-of-thumb model of thermal power plant uptake and release is developed and implemented to estimate the power generation impact.

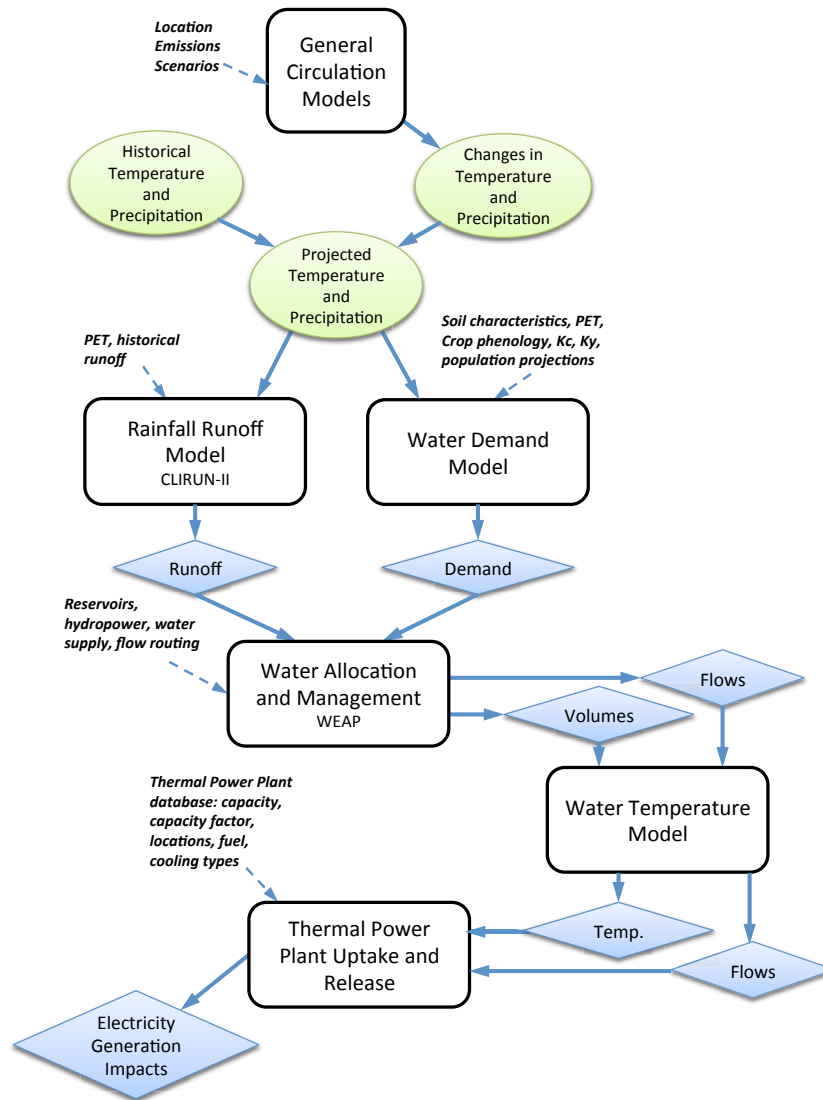


Figure 1. Model overview diagram.

2.1 Climate Scenarios

For the baseline climate scenario, the model is forced by Princeton University’s publicly available Global Meteorological Forcing Dataset for land surface modeling (Sheffield *et al.*, 2006) specified at a $0.5^\circ \times 0.5^\circ$ resolution for 1980–2008. We spatially interpolate the climatological data within the $0.5^\circ \times 0.5^\circ$ grid to each HUC’s centroid. We assume uniform

conditions throughout the entire HUC. Daily minimum and maximum air temperature, T_{min} and T_{max} , respectively, are defined on a $1^\circ \times 1^\circ$ scale and we adjust the interpolation accordingly.

Climate projections and future time periods (henceforth referred to as eras) allow us to estimate the benefits of GHG mitigation and how those benefits evolve over time. First, we develop a control scenario that represents present day climate conditions but includes population projections. We then alter the control scenario input data by changes in future climate, and measure the resulting changes in output across the various scenarios. Detailed descriptions of the global GHG mitigation scenarios used in this analysis, along with a comparison to the representative concentration pathways (RCPs) and global climate projections, are provided in Paltsev *et al.* (2013) and Waldhoff *et al.* (2014). In short, three emission scenarios are used: a reference (*REF*) or ‘business as usual’, and two scenarios representing futures with policies that limit global GHG emissions such that total radiative forcing levels in 2100 are stabilized at 4.5 W/m^2 (*Policy 4.5*) or 3.7 W/m^2 (*Policy 3.7*). The *REF* scenario has a total radiative forcing of 10.0 W/m^2 in 2100. Using the IPCC simplified equations, the *REF* has a total radiative forcing of 8.8 W/m^2 , and is therefore similar to representative concentration pathway (RCP) 8.5. The base framework used to project future climate, the Community Atmospheric Model linked with the MIT Integrated Global Systems Model (IGSM-CAM), is presented in Monier *et al.* (2013, 2014), which also provide a summary of the simulations and details on the regional projections of climate change used in this study. Since the IGSM-CAM study only considers one GCM, the IGSM pattern scaling approach was used to develop a balanced set of regional patterns of climatic change for CONUS (see Monier *et al.* 2014 for methodological details). This approach preserves all the CIRA economic and emissions results, but replaces the CAM climate projections with projections based on the spatial patterns of alternative GCM-EHCBS. Two GCMs were chosen for the pattern-scaled results, each with very different patterns of change over CONUS: the Model for Interdisciplinary Research on Climate (MIROC3.2-medres) projects drying and strong warming, and the Community Climate System Model (CCSM3.0) projects more moisture and less warming than MIROC. Monier *et al.* (2014) discusses how the IGSM-CAM simulations compare to the pattern-scaled MIROC and CCSM projections, as well as the limitations of both methods. Since the IGSM-CAM climate projections are similar to the pattern-scaled CCSM, we present the IGSM-CAM results and the pattern-scaled MIROC results in this paper.

The climate projections for each of the GHG mitigation scenarios are split into four eras: 2025, 2050, 2075, and 2100. Each era is represented by daily climate variability (sourced from Sheffield *et al.*, 2006) with changes in climate applied. For precipitation, we use a simple ratio method where the change in precipitation is expressed as the future monthly mean precipitation divided by the historical monthly mean precipitation. For temperature, we use a simple “delta” method, where changes in temperature are expressed as differences between the mean monthly modeled historical temperature and projected future temperature. The primary climate projections in this analysis assume a climate sensitivity of 3°C (denoted as *CS3*); to evaluate the effect of higher climate sensitivity levels, two projections assume a sensitivity of 6°C (*CS6-REF*)

and *CS6-Pol3.7*, which use emissions from the *REF* and *Policy 3.7* emission scenarios, respectively). Additionally, we run three years: the year with the median runoff, 10th percentile runoff, and 90th percentile runoff, calculated for each hydrologically independent basin. For the remainder of the paper, we name these the median, wet, and dry climate years, respectively.

2.2 Runoff Model

The climate projections for each emission scenario were used to develop monthly runoff estimates. Runoff modeling converts the climate changes into changes in surface water availability—important for the water resource model. Surface water runoff was modeled with the rainfall-runoff model CLIRUN-II (see Strzeppek *et al.*, 2011, 2013), the latest available application in a family of hydrologic models developed specifically for the analysis of the impact of climate change on runoff (first proposed by Kaczmarek, 1993). CLIRUN-II models runoff with a lumped watershed defined by climate inputs and soil characteristics averaged over the entire watershed, simulating runoff at a gauged location at the mouth of the catchment on a monthly time-step.

CLIRUN-II has adopted a two-layer approach following the framework of the SIXPAR hydrologic model (Gupta and Sorooshian, 1985). A unique conditional calibration procedure was used to determine the coefficient values that characterize each of the 2,119 catchments. This procedure optimizes via a pattern search algorithm developed by MATLAB, minimizing the sum of square errors of the simulated and observed runoff. As no naturalized runoff dataset for the 8-digit HUCs of CONUS is currently available, the observed runoff data used to calibrate CLIRUN-II was based on naturalized runoff data for 99 basins of CONUS from USWRC (1978). To calibrate each 8-digit HUC, the runoff within each of these 99 basins was allocated to the underlying 8-digit HUCs based on mean annual 1971 to 1980 precipitation that was spatially averaged from the $1/12 \times 1/12$ degree PRISM dataset (PRISM, 2014).

Although we have confidence in the calibration runoff dataset at the resolution of the 99 basins, downscaling these data to the 2,119 8-digit HUC introduces uncertainties. An alternative to using a calibrated rainfall runoff model would have been to rely on a routing model such as the Variable Infiltration Capacity (VIC) or Soil Water Assessment Tool (SWAT) tools that are capable of simulating runoff without calibration. The aggregated runoff outputs from these models could be validated and then ‘tuned’ using the 99 basin outflows, but no assurances exist that the runoff at the 8-digit resolution will fit naturalized observations. Efforts at the U.S. Geological Survey (USGS) are currently underway to develop an improved naturalized runoff dataset for the U.S. (e.g. Farmer and Vogel, 2012), although a CONUS-wide dataset is far from complete.

2.2.1 Water Demands

Water demands are the other side of the water balance, and are developed using 2005 data from USGS on annual water withdrawals and consumptive use in a range of sectors including irrigation, municipal and industrial (M&I) use, mining, thermal cooling, and several other sectors (Kenny *et al.*, 2009). These data are available at the 3,109 counties of CONUS, which were

spatially averaged to the 8-digit HUC resolution using the same approach taken by the U.S. Forest Service in their development of the Water Supply Stress Index (WaSSI) (USFS, 2014). For all sectors but irrigation, we assumed that withdrawals were constant each day of the year, such that monthly withdrawals are apportioned from yearly values based on the number of days in each month.

Base monthly 2005 irrigation withdrawals were developed by allocating the total annual withdrawals (from USGS) according to the total irrigation water requirements (IWRs) of the irrigated crop mix in each HUC. IWRs were based on the meteorological dataset described above (Sheffield *et al.*, 2006), irrigated crop area estimates from the 2008 Farm and Ranch Irrigation Survey (USDA, 2010), and estimates of irrigation water depth requirements for each crop using methods developed by the U.N. Food and Agriculture Organization (FAO) (Allen *et al.*, 1998). The FAO method requires estimates of potential evapotranspiration (PET), which were calculated using the Modified Hargreaves approach (Droogers and Allen, 2002). This procedure generated a base time series of 29 years (1980 to 2008) of irrigation water requirements that vary on a monthly basis, with the 2005 annual totals summing to USGS data for each 8-digit HUC. Water requirements for each of the future eras and under each emission and climate scenario were driven by the FAO method, which vary based on both PET and precipitation under each scenario. As a result, total CONUS irrigation withdrawals in each era-scenario combination vary from 2005 levels.

2.3 Water Resources Management Model

We then simulate reservoir management and routing using a water resources systems model, where the simulated runoff—used as surface water supply—and projected water demands are used to optimize water allocation based on a prescribed set of priorities. This model is an adaptation of the Water Evaluation And Planning (WEAP) model (Sieber and Purkey, 2007), a well-established river basin system modeling software. This version was rewritten in the MATLAB language for computation speed and automation, but remains methodologically consistent with the WEAP model, described in detail in the WEAP documentation.

The WEAP model simulates the sequence of existing and planned reservoir activity and demand nodes along the system. Three demand types, or nodes, are modeled throughout the system, which are in competition for water dependent on the sequence (upstream/downstream). The node types are municipal and industrial (M&I) water use, hydropower generation, and irrigation withdrawal. The hydrologic boundaries used to define the basins are the 2,119 8-digit HUCs of CONUS. The structure of each basin is generic, prescribed with input characteristics that are unique to each HUC. Reservoir data, such as locations, hydropower capabilities, and the information needed to calculate surface area and volume are all retrieved from the Army Corps of Engineers (Corps, 2013). Hydropower production is calculated and calibrated to the National Renewable Energy Laboratory (NREL) Regional Energy Deployment System (ReEDS) model (Short *et al.*, 2011). For each of the basins, the priorities of the various water users are assumed to be in the following order: (1) minimum flows driven by environmental and trans-boundary

concerns, (2) M&I water demands (including mining and thermal cooling), (3) irrigation demands, and (4) hydropower production.

2.4 Model of Water-body Temperature

The model is constructed in three parts. First we build the river network to specify the sequence of flow for each 8-digit HUC. Second, we build geometries and characteristics for each HUC's representative river reach. The third step is to initiate river temperatures and model the atmospheric heat exchange for the specified time period.

2.4.1 River Network

To build the river network we used the Enhanced River Reach File (erfl) from USGS, which is the EPA's digital record of over 60,000 river reaches in the United States, intended for national water-quality modeling. For each river segment, the data set contains corresponding parameters, outlined in **Table 1**. Using these parameters we build the river network.

The river network is both a network of HUCs and rivers within the HUCs. The river segments are on average 16km long, and each HUC contains approximately 30 river segments. Only 6 or 7 river segments form the main river that spans each HUC, and the rest are side branches feeding into the main segment. For two river segments that connect, they will have a matching Tnode and Fnode; each river segment runs from the Tnode (uppermost point) to the Fnode (lowermost point). To create the network of HUCs, we exhaustively search each HUC to find all nodes that connect one HUC to another, and for each HUC we store the downstream HUC 8-digit ID. We choose only the main river segments that connect the top of each HUC to the bottom. This involves tracing down each river segment, and choosing the largest flow river segment when a fork is encountered. Creating the network of HUCs also requires specifying the order of each HUC (i.e. the order it should be run). The atmospheric heat exchange component of the model requires upstream temperatures to be fed into the system and outputs downstream temperatures; therefore, the order in which the HUCs are modeled is important. If a HUC has no upstream HUC then its order is set to 1. For all other HUCs their order is one larger than their upstream HUC. If two HUCs merge into one then the order of the downstream HUC is specified to be one more than the highest ordered upstream HUC. The majority of the HUCs are of order 1, with many HUCs feeding directly into the ocean. About 15% of the HUCs are of order 2, and while the number of HUCs with higher orders quickly diminishes, there remain some long sequences, the largest being 30 HUCs long from the uppermost reach to the ocean.

2.4.2 River Geometry

The same erfl data set (see Table 1) used for the network is also used to construct the representative river reaches. We use the data parameters for the river segments from this dataset that form the main river segment for each HUC.

We construct the representative river reach dimensions. The length is the sum of all lengths of river segments used for the main river in the HUC. We assume each river bed is parabolic and solve for width, depth and cross-sectional area in terms of river reach mean flow, Q , in cubic

meters per second, following Leopold and Maddock (1953). The width of the river reach in meters, B , is defined as

$$B = 2.71 Q^{0.557} \quad (1)$$

the mean depth of the river reach in meters, H , is defined as

$$H = 0.349 Q^{0.341} \quad (2)$$

and the cross-sectional area in square meters, A , is defined as

$$A = \left(\frac{2}{3}\right) B D \quad (3)$$

2.4.3 Heat Budget Model

The initial conditions for water temperature are approximated using the Stefan and Preud'homme (1993) method, defined by three regionally specific constants, α_s , β_s , and Y_s (henceforth referred to as Stefan-Preud'homme Constants), as well as the mean air temperature of the previous 7 days, $\overline{T_a}$, as follows.

$$T_1 = \frac{\alpha}{1 + e^{\gamma(\beta + \overline{T_a})}} \quad (4)$$

Temperature is then tracked within the model using a heat budget model approach (Chapra, 1997), that simulates the surface heat exchange of a body of water as well as water sources/sinks through inflows from upstream basins, outflows downstream, small tributaries, and groundwater. The governing heat budget equation is as follows:

$$V\rho C_p \frac{dT}{dt} = A_s J + Q_{in}\rho C_p T_{in} - Q_{out}\rho C_p T \quad (5)$$

where V is volume, ρ is water density, C_p is specific heat, T is temperature, t is time, A_s is surface area of the water body, J is the total heat exchange through the air-water interface, Q_{in} and Q_{out} are the flows into and out of the system, respectively, and T_{in} is the temperature of Q_{in} . Q_{in} includes both upstream flow into the reach as well as additional runoff from surface and baseflow. We assume that the runoff temperature is flowing into the reach at the temperature calculated using the Stefan-Preud'homme Constants, same as the initial condition temperature. We model this differential equation using a predictor-corrector approach as outlined in MacCormack (1969), which has the advantage of stability and is not plagued by numerical dispersion.

In the summer, as temperature warms and solar radiation increases, stratification in temperate reservoirs occurs. Temperature during the season of stratification is modeled differently for reservoirs, where a two-layer model is used, representing both the *epilimnion* (top) and the *hypolimnion* (bottom) layers. For example, if the reservoir is bottom-releasing (i.e. outflow is occurring in the hypolimnion) then the following is used to model the reservoir temperature (Chapra, 1997):

$$V_e \rho C_p \frac{dT_e}{dt} = A_s J + Q_{in} \rho C_p T_{in} + v_t A_t \rho C_p (T_h - T_e) \quad (6)$$

$$V_h \rho C_p \frac{dT_h}{dt} = -Q_{out} \rho C_p T_e + v_t A_t \rho C_p (T_e - T_h) \quad (7)$$

Where the subscripts e and h represent the epilimnion and hypolimnion, respectively; v_t is the thermocline heat transfer coefficient; and A_t is the thermocline area. v_t is estimated using the relationship developed by Snodgrass (1974).

The surface heat exchange, J , is the sum of five energy flux components including evaporation (J_e), conduction (J_c), water longwave radiation (J_{br}), atmospheric longwave radiation (J_{an}), and solar radiation (J_{sn}). Each is calculated as follows.

The river loses heat to the evaporation process. This component is therefore subtracted from the total heat surface flux. The evaporation term is calculated as

$$J_e = f(U)(e_s - e_{air}) \quad (8)$$

where $f(U)$ is a function of wind defined as

$$f(U) = 19 + 0.95 U^2 \quad (9)$$

e_s is the saturation pressure, corresponding to surface temperature, which we take to be the average temperature of the incoming water:

$$e_s = \frac{4.596e^{17.27T_w(n-1,h-1)}}{237.5+T_w(n-1,h-1)} \quad (10)$$

e_{air} is the vapor pressure of air defined as

$$e_{air} = \frac{SH(h) SP(h)}{0.622} \quad (11)$$

and e_{sat} is the saturation pressure defined to be

$$e_{sat} = 4.596 e^{\frac{17.27+T(h)}{237.3+T(h)}} \quad (12)$$

Conduction occurs when there is a temperature difference between the river and air, and is accelerated with wind. The conduction term is defined as

$$J_c = c_1 f(U)(T_w(n-1, h-1) - T(h)) \quad (13)$$

If water is colder than air, this is a negative term; therefore, this term is subtracted from the total heat flux.

Water longwave radiation is the energy leaving the river, primarily dependent on the river's temperature. The warmer the river, the more energy lost to the atmosphere through longwave radiation. This term will therefore also be subtracted from total energy balance.

$$J_{br} = E\sigma(T_w(n-1, h-1) + 273)^4 \quad (14)$$

Similarly to water longwave radiation, the energy in the atmosphere increases with temperature and radiates outwards. The amount absorbed by the river is a function of not only the amount of atmospheric longwave radiation but also the reflectivity and absorptive capacity of the water. It is defined as

$$J_{an} = \sigma(T(h) + 273)^4 (A + 0.031\sqrt{e_{air}})(1 - R_1) \quad (15)$$

Solar radiation is provided as a daily average in the data used for this model. In reality, solar radiation varies throughout the day based on variables such as solar angle and cloud coverage. We approximate the hourly solar radiation using a sinusoidal function, where the daily average is

consistent with the mean solar average for that data listed in the Princeton Dataset. We then approximate a reflection coefficient, R_h , based on the time of day and assumed solar angle from Brown and Barnwell (1987), taken from Chapra (2008).

$$J_{sn} = (1 - R_h)SOL(h) \tag{16}$$

Each segment is modeled as ten sub-segments, equally split by segment length, each with a unique water temperature and modeled boundary interactions, both advection and dispersion. The uppermost sub-segment (i.e., the upper boundary) temperature is set to the upstream temperature. The middle eight sub-segments are modeled as described above and the lower boundary is estimated as

$$T_M = 2 * T_{M-1} - T_{M-2} \tag{17}$$

2.5 Power Plant Model

In order to project the effect of climate change on thermal power generation, we link a database of thermal power facilities (EW3 database from the Union of Concerned Scientists (UCS, 2012)) to the 8-digit HUC resolution. Annual Generation by the four major fuel types modeled is shown in **Figure 2**.

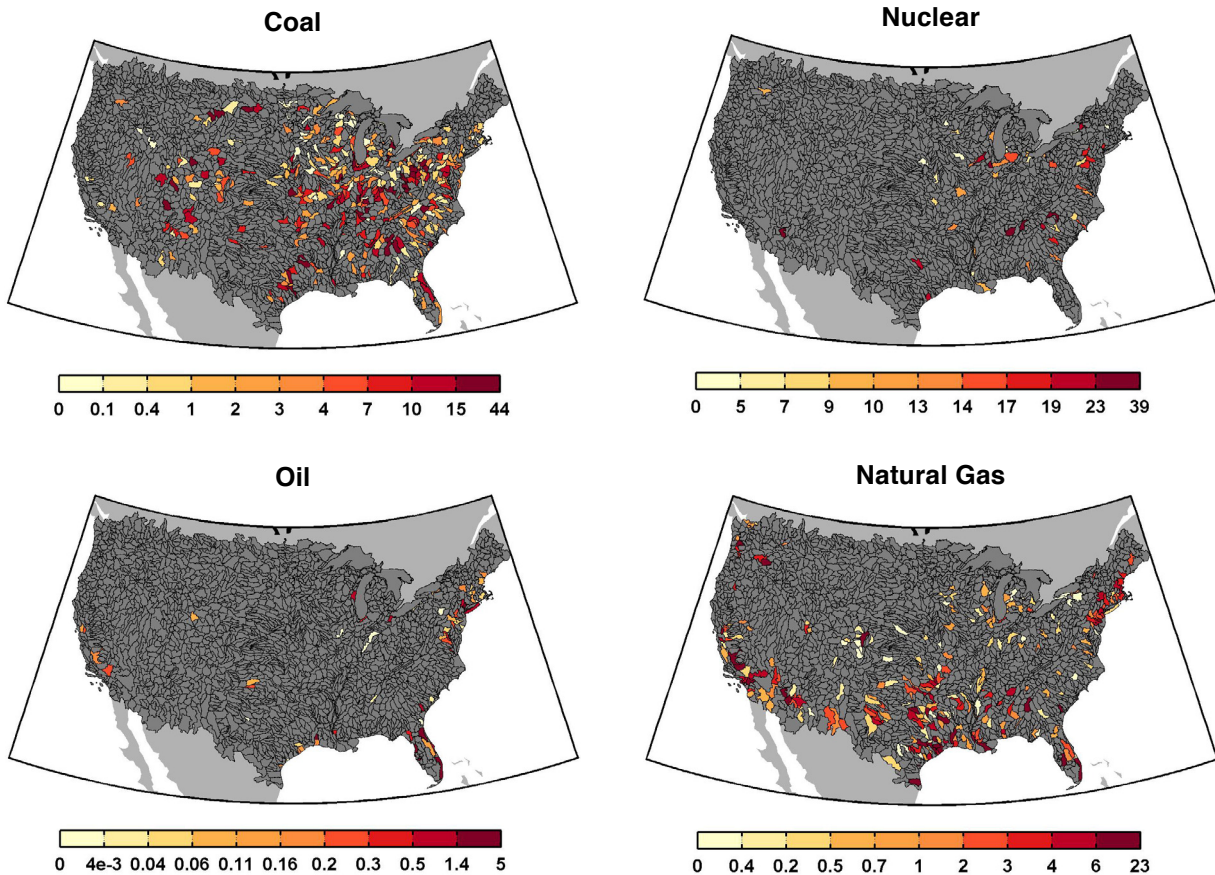


Figure 2. Annual generation (in TWh) for coal, nuclear, oil, and natural gas.

Environmental policies regulating power plant withdrawals and releases vary state to state. For this study, we apply commonly used regulation types: withdrawal, near-field temperature, and far-field temperature. Withdrawal refers to a limit on the fraction of the flow that can be withdrawn from the river. The near-field temperature refers to the temperature of water near the release, before sufficient mixing has occurred, and far-field temperature refers to the water temperature further downstream of the release, after the effluent has been fully mixed. We use conservative regulations as follows: withdrawal is limited to less than ½ of the flow; near field temperatures are to not exceed 5.6°C warmer than the original water temperature after ½ of the of the river has mixed; and far-field temperatures are to not exceed 32°C.

In order to apply these regulations, we first need to estimate the water demands of the power plant. For once-through cooling plants, the procedure is straightforward. We can calculate the heat rejection in cooling water (*HEAT*), when the plant is running at capacity, as

$$HEAT = CP(1 - E - \delta)/E \quad (18)$$

where *HEAT* is measured in kJ/s, *CP* is the total power plant capacity in kW, *E* is the thermal efficiency, and δ is the portion of heat lost to in-plant and stack losses (Adams and Harleman, 1979). We assume that thermal efficiency and in-plant and stack losses are constant and refer to values in EPRI (2002).

The amount of flow needed to remove this heat is

$$Q_{demand} = \frac{HEAT}{c_p \rho (T_{out} - T)} \quad (19)$$

where T_{out} is the effluent temperature and T is the water temperature in the river before the effluent release. We assume that the temperature coming out of the plant is 11.2°C warmer than the water going into the plant, thus the difference between T_{out} and T is 11.2. We can then calculate near-field and far-field temperatures at each hour and determine the amount of water the power plant can withdraw without violating the regulation.

Thermal power plants with cooling towers and cooling ponds also withdraw water to make up for evaporation and to avoid the buildup of salts and solids. Estimating these withdrawals is more complicated. For this reason, we use values of withdrawal per MWh generated as reported in EPRI (2002). With these rates, we can estimate the power plant demand and apply our withdrawal regulation. **Figure 3** shows the total annual generation for each HUC by cooling technology.

Finally, we calculate the fraction of regulated withdrawal over demands for each power plant. This fraction is used as an indicator of the climate change impacts. Note that, for once-through cooling plants this fraction implicitly assumes the plants prefer to generate at full capacity over the year. In reality, this is not the case due mostly to varying electricity demand and price, as well as grid system management; capacity factors for once-through plants have a calculated median of 0.55, with the majority of the plants ranging from 0.26 to 0.69 (the 25th and 75th percentiles, respectively). Nonetheless, the allowable withdrawal fraction is an accurate indicator of the time during the year when the plant will not violate environmental regulations, a value that will likely impact generation if this fraction either increases or decreases in the future. One can

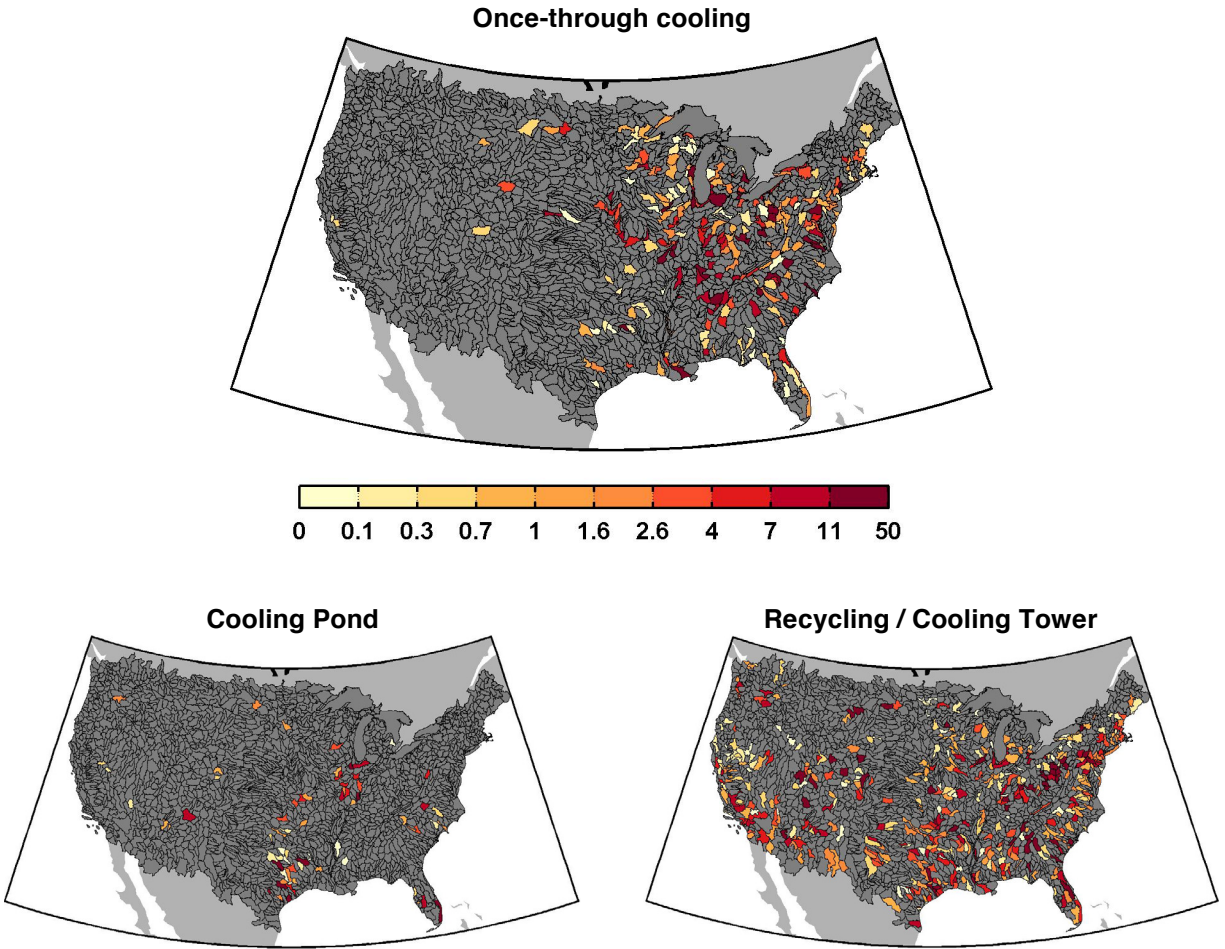


Figure 3. Total annual generation (in TWh) for three cooling technologies: once-through cooling, cooling pond, and recycling.

also view this value as a measure of changes in availability; i.e. if the fraction decreases, the plant is more likely to have restricted withdrawal when the plant is needed to generate electricity (as dispatched by a grid operator), thus requiring a more expensive alternative plant to generate the needed electricity.

3. MODEL VALIDATION

USGS provides river temperature output for multiple river stations throughout the U.S. This river temperature dataset is used to validate the model. The model is first validated and calibrated for a detailed river reach with measured USGS hourly flow and temperature. We use the Delaware River for this, where the standalone river temperature model is used. The model is next evaluated at 16 stations with sufficient daily temperature data, where the full model system is used, the same framework used to later evaluate the climate change effects and GHG mitigation benefits.

3.1 The Delaware River

We validate the physical model of the rivers' heat transfer by testing the model against a detailed flow model of the Delaware River. We choose a 190km reach of the Delaware that has well measured temperature and flow data, and no dams upstream. The section of the river that we use to test the model is shown in **Figure 4**.

We use Princeton atmospheric data, and the USGS Delaware River hourly upstream flow data from 2008 to force localized climate conditions and upstream flow and temperature conditions. We apply an upstream river temperature boundary condition based on air temperatures and Stefan-Preud'homme Constants, and apply the Princeton atmospheric data for wind, humidity, and pressure. Running the model we obtain river temperatures at the downstream portion of the river segment and compare them with measured temperatures. The results are presented in **Figure 5**.

Since the summer months (June, July and August) are of critical importance for power plant operations, we show the model results for summer months in **Figure 6**. We end up with an R^2 of 0.8764 for hourly measurements and an R^2 of 0.89 for daily measurements.



Figure 4. The left map is of the Delaware River and coastline. The right map includes the entire section of the river used to test the model.

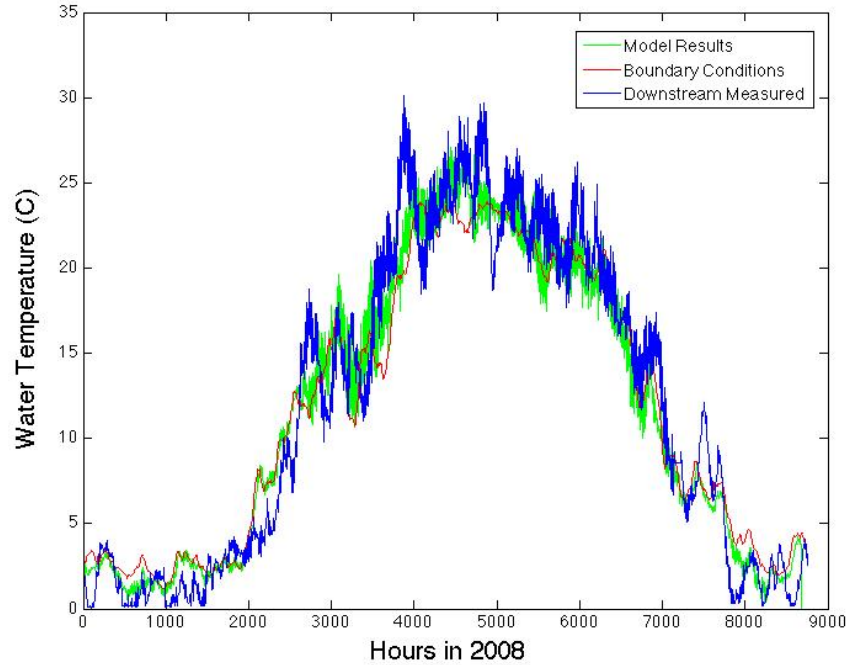


Figure 5. Hourly water temperature results for upstream boundary temperatures using Stefan-Pred'homme Constants (red), downstream modeled temperatures (green) and measured downstream temperatures (blue).

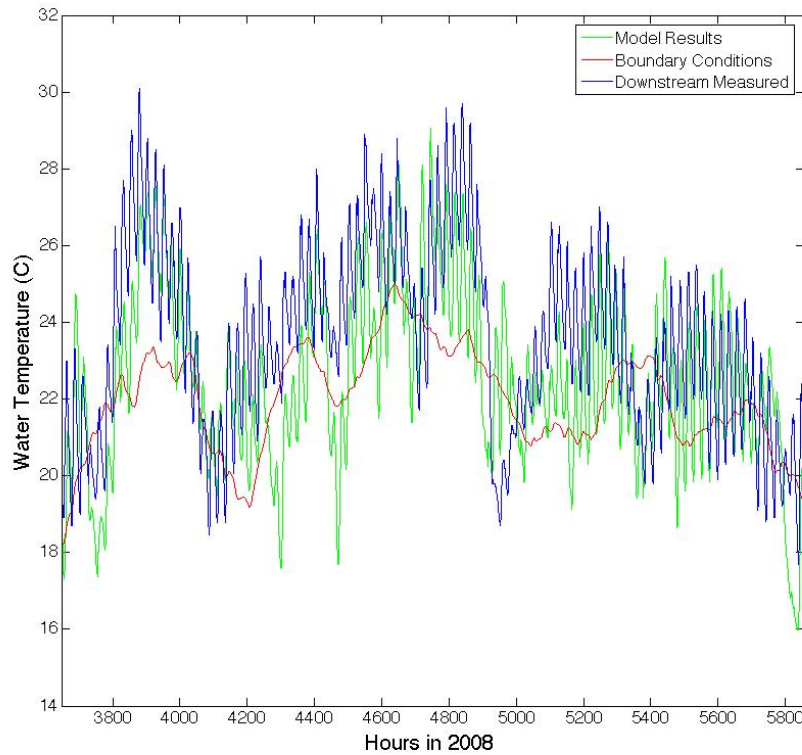


Figure 6. Summer water temperature modeling results of downstream measured temperatures (blue), modeled temperatures (green) and upstream boundary temperatures using Stefan-Pred'homme Constants (red).

3.2 Multi-HUC Model Testing

We select 17 HUCs with hourly station temperature data for the whole of 2008 and compare our model results with the measured temperatures. In this case, we use flow outputs from the water resource management model described previously, which outputs managed streamflow. **Figure 7** shows the results for these HUCs. Statistics and information about these stations are shown in Table 1 and the locations are shown in **Figure 8**. These locations represent a variety of locations throughout the U.S., as well as a variety of flows and hydrologic reach orders. R^2 values range from 0.68 to 0.93, with a median of 0.88. Given that these river temperatures were estimated at the back end of a number of models (climate, runoff, water demands, water management), all contributing uncertainty and error, we find that the model performs with reasonable accuracy.

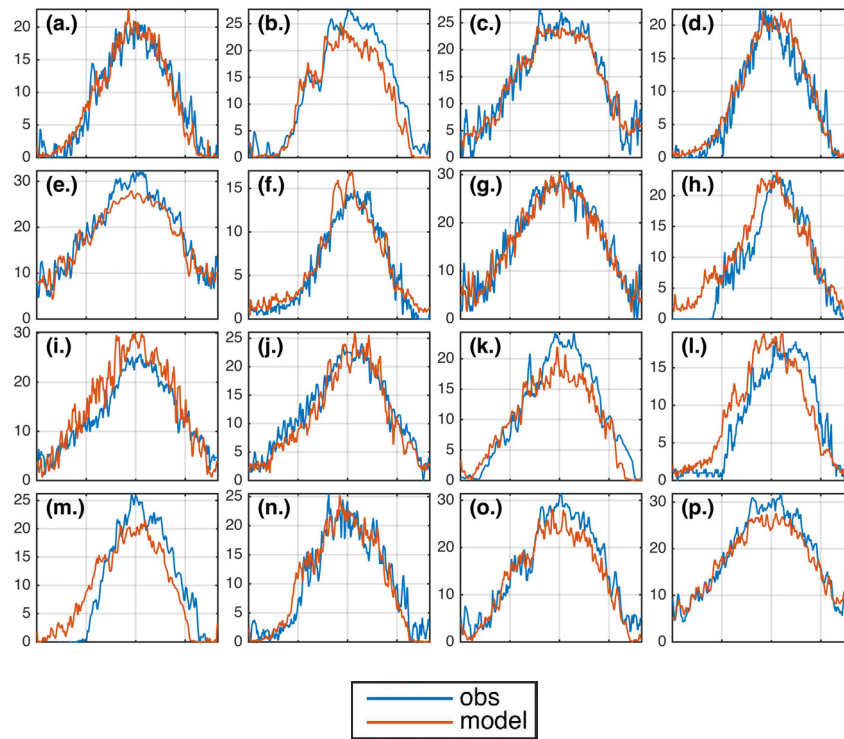


Figure 7. Observed (blue) and modeled (red) daily river temperatures for the 16 locations used.

Table 1. Validation information.

Fig	Name	HUC ID	R^2	Fig	Name	HUC ID	R^2
(a.)	Au Sable	4070007	0.91	(i.)	Lower Virgin	15010010	0.68
(b.)	Lower Allegheny	5010009	0.88	(j.)	Truckee	16050102	0.87
(c.)	Upper Clinch	6010205	0.93	(k.)	Lower Klamath	18010209	0.84
(d.)	Namekagon	7030002	0.91	(l.)	Upper Connecticut	1080101	0.75
(e.)	Deer-Steele	8030209	0.88	(m.)	Lower Penobscot	1020005	0.80
(f.)	Arkansas Headwaters	11020001	0.91	(n.)	Mid. Del.-Mongaup-Brodhead	2040104	0.89
(g.)	Middle North Canadian	11100301	0.89	(o.)	Middle Potomac-Catoctin	2070008	0.87
(h.)	Lower Yampa	14050002	0.82	(p.)	Lower Broad	3050106	0.91

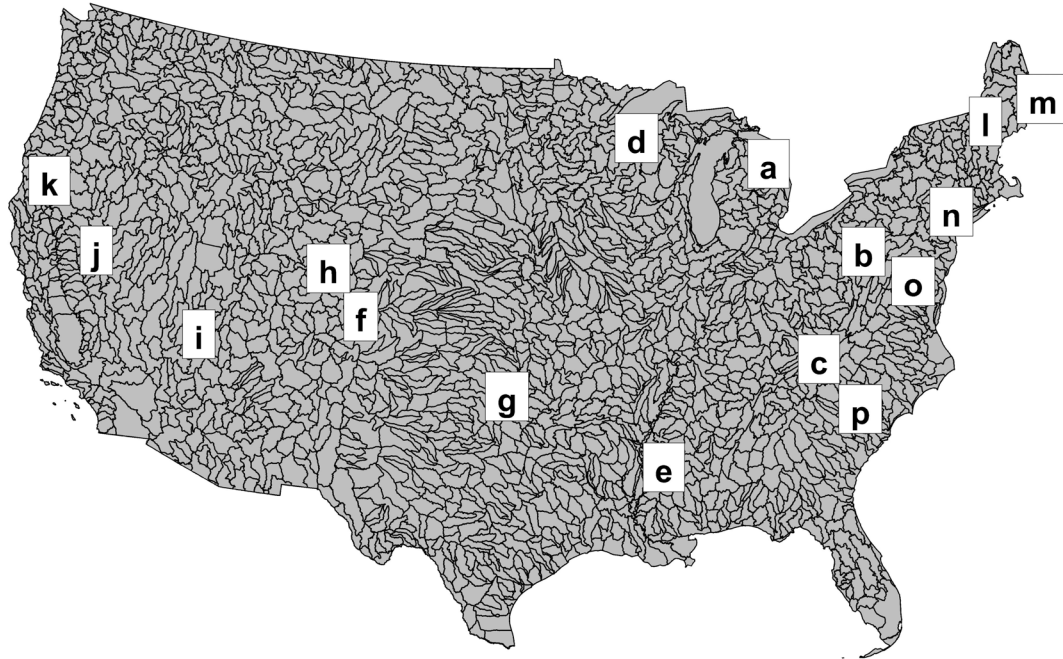


Figure 8. Locations of the river temperatures used for validation.

4. RESULTS

In this section, the results from the various scenarios are presented using three major indicators of climate change impacts: surface water availability, water temperature, and the fraction of time during the year that existing thermal power plants exceed river temperature regulations on uptake and release. The baseline is shown first for these indicators followed by the changes from the baseline, and we conclude with the mitigation benefits.

4.1 Baseline

Baseline water temperature for four seasons of the year is shown in **Figure 9** for the baseline median climate year. In the Dec-Jan season, mean water temperatures are close to 0°C for much of northern CONUS, with warmer temperatures in the south, especially in southern Florida where mean water temperature exceeds 20°C. The Jun-Aug season is considerably warmer, with most of the north and high-elevated regions exceeding 20°C, and the southern regions exceeding 30°C. **Figure 10** shows the seasonal mean flow for the baseline median climate year. In this figure, we see somewhat consistent flow patterns across seasons, although there are a few regions that are season dependent, e.g. flows in the northwest are higher in Mar-May than Jun-Aug.

In order to summarize the power uptake restrictions caused by the environmental regulations imposed, we show the percentage of power plants as well as the total generation that falls into one of two categories: (i) no power plant restriction or (ii) withdrawal restriction (**Table 2**). As shown, power plants with once-through cooling technologies are most often restricted, with only 58% of the plants having no restrictions in the baseline scenario. While plants with cooling

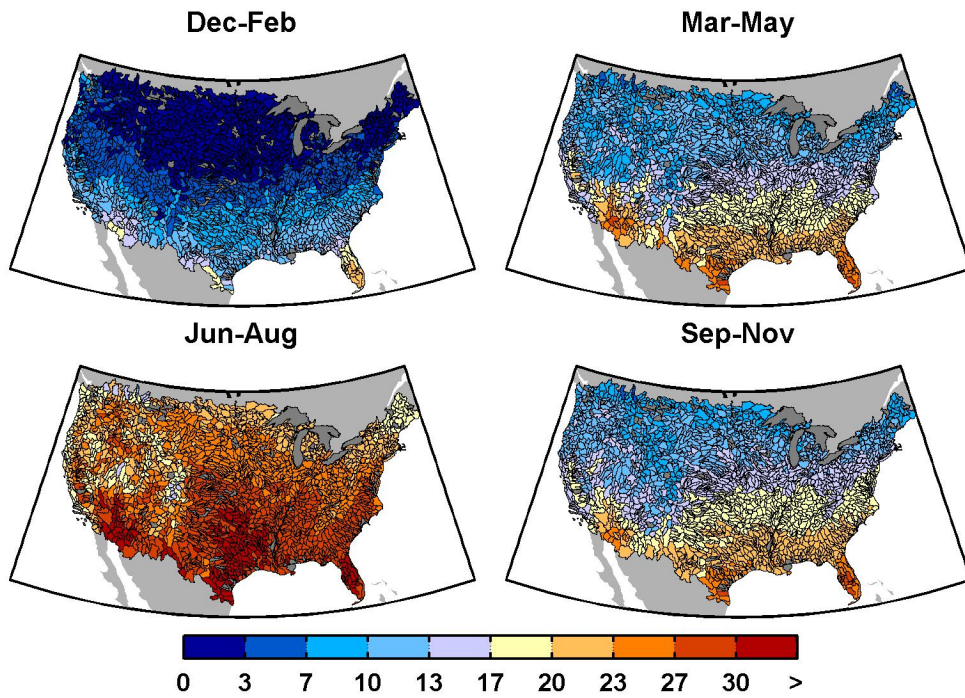


Figure 9. Mean seasonal baseline surface water temperatures at the HUC-8 scale (°C).

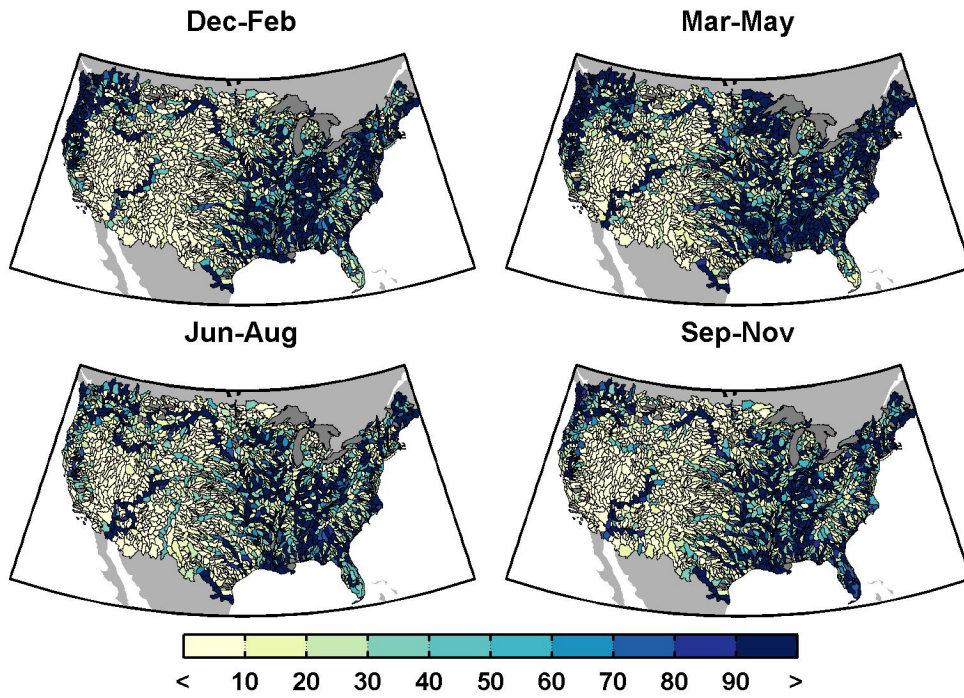


Figure 10. Mean seasonal baseline river flows in cubic meters per second.

Table 2. Percentage of power plants and total generation (in TWh) in two categories based whether or not the power plant is restricted by the environmental regulations imposed.

		No Restriction		Restricted	
Cooling Tech.	Once-Through	59%	623.4	41%	359.4
	Cooling Tower	94%	2687.0	6%	112.9
	Cooling Pond	98%	242.5	2%	0.7
Fuel Type	Coal	77%	1218.5	23%	320.8
	Natural Gas	90%	1077.5	10%	116.1
	Nuclear	72%	165.5	28%	38.3
	Oil	88%	198.6	12%	25.7

towers make up the majority of annual electricity generation, they are less likely to be restricted because they require less withdrawal for cooling. Also, note that we will not see improvements in the future for plants that do not have restrictions in the baseline since the allowable withdrawal fraction is already at the maximum—one. This means that once-through cooling plants have more capacity for future increases in the allowable withdrawal fraction than do plants with cooling towers. In terms of the fuel type, nuclear plants are most likely to be restricted, followed by coal plants; however, the restricted coal plants represent a larger portion of annual generation than nuclear.

4.2 Future Changes

Now we look specifically at changes in water temperature, flow, and withdrawal restriction for CONUS. For these, we display the differences in the results, comparing the various emissions scenarios to the control scenario (no changes in climate) to measure the climate change impact. **Figure 11** shows the changes in water temperature by 2050 for two policy cases—*CS3-REF* and *CS3-POL3.7*—as well as the two GCMs—IGSM-CAM and MIROC. As shown, water temperature varies by magnitude and geographic location. *CS3-REF* is always warmer than the stringent mitigation case, *CS3-POL3.7*, though the variation across HUCs is driven more by GCM than mitigation policy—IGSM-CAM shows larger increases in temperature in the west, while MIROC shows larger increases in temperature in the Great Plains. These changes in water temperature are influenced by changes in climate as well as changes in flow.

Figure 12 shows the projections of changes in streamflow in 2050 for the same four scenarios. We see that the IGSM-CAM results in considerably higher streamflow than MIROC, and again the geographic variation is driven more by GCM than by mitigation policy. In fact, the differences between mitigation policies are different in sign for the two GCMs: compared to *CS3-REF*, MIROC mostly results in streamflow increases for *CS3-POL3.7*, whereas IGSM-CAM mostly results in streamflow decreases.

These changes in water temperature and streamflow then influence the allowable uptake for thermal power plants, as implemented in the power plant model described previously. Changes in allowable withdrawal for 2050 are shown for the same four scenarios, again as the change

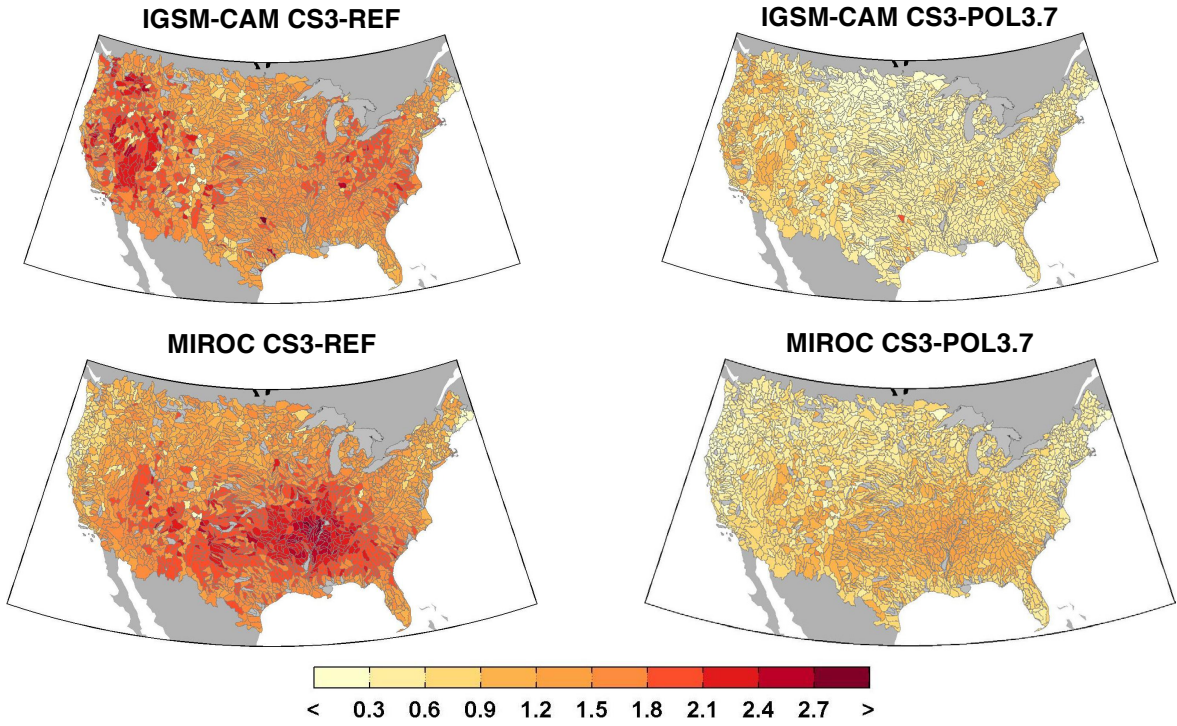


Figure 11. Change in Temperature ($^{\circ}\text{C}$) from the control scenario in 2050.

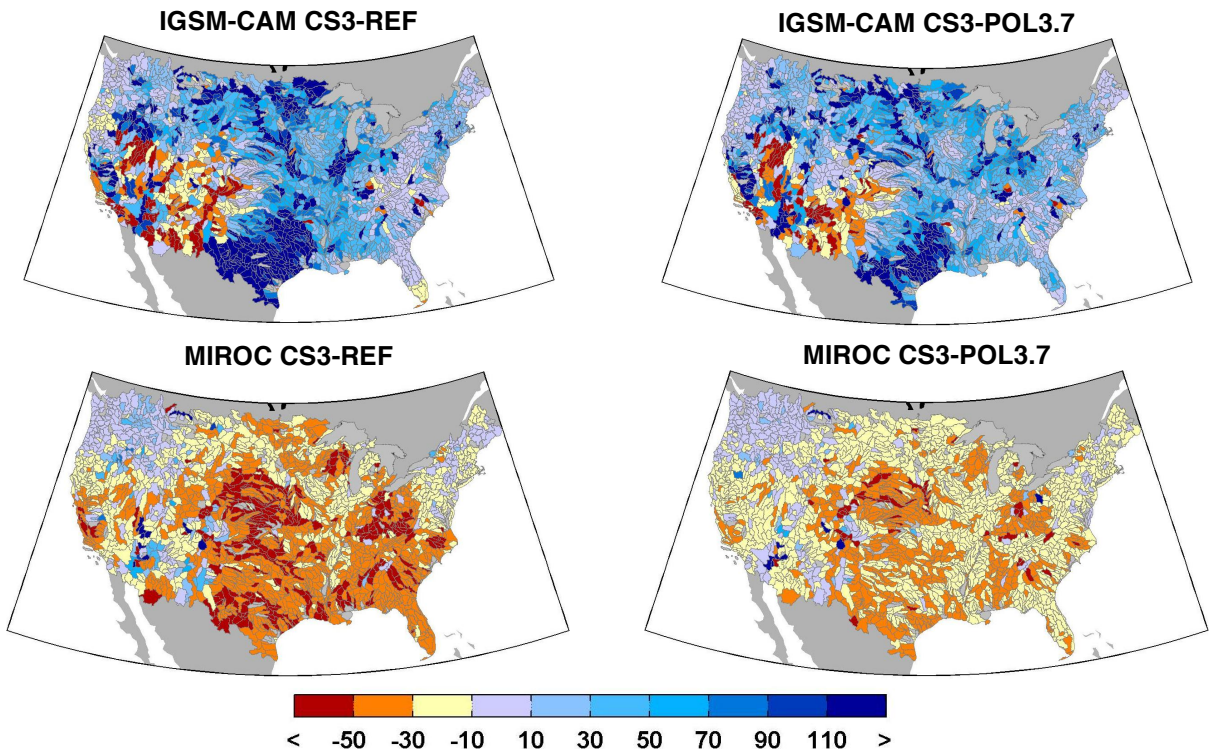


Figure 12. Change in Flow (percent) from the control scenario in 2050.

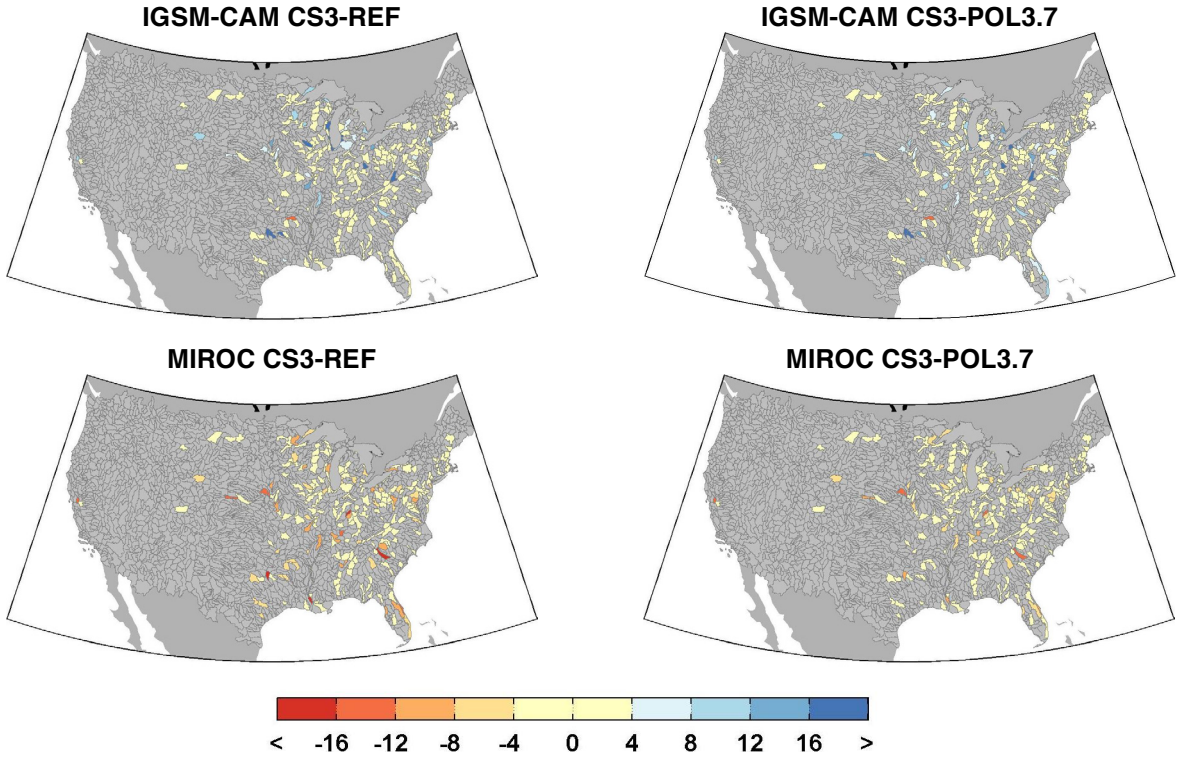


Figure 13. Changes in withdrawal allowed for HUCs with once-through cooling technology in 2050.

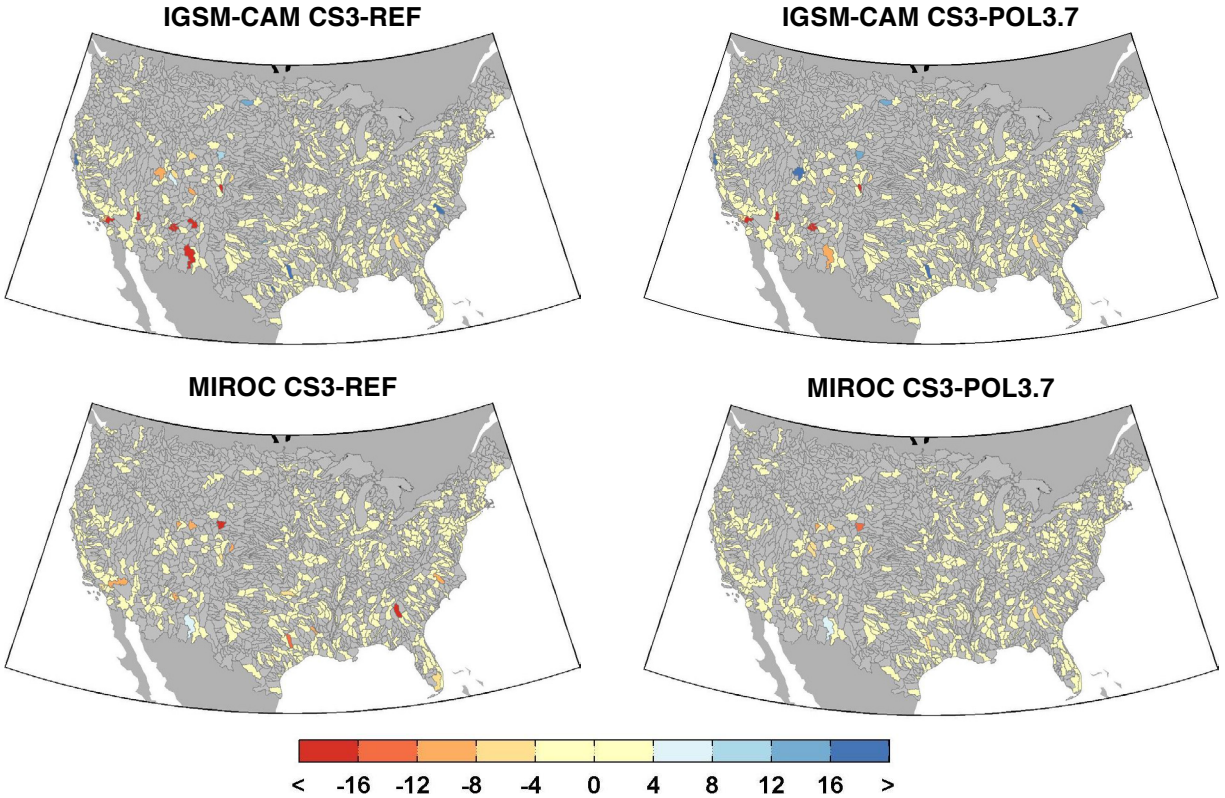


Figure 14. Changes in withdrawal allowed for HUCs with recirculating cooling technology in 2050.

from the control scenario for once-through cooling plants in **Figure 13** and for plants with cooling towers in **Figure 14**. As expected, once-through cooling plants are more sensitive to changes in climate than plants with cooling towers. Also, note that the GCM projections of changes in flow play a major role in these values. There are less once-through cooling plants in the west where water is more scarce. Since IGSM-CAM is projecting a hotter and drier climate in the west, and a relatively cooler and wetter climate in the east, once-through cooling plants conditions improve in the future. MIROC projects a drier and considerably hotter climate in the east and mid-west, causing a substantial decrease in allowable withdrawal for once-through cooling plants.

In **Figure 15**, we show the total changes in allowable withdrawal for all cooling technologies, future scenarios, and separate out the dry, median, and wet climate years. Note that the total generation from the plants considered is over 3,200 TWh annually. Using national energy prices (\$90/MWh, in 2005 USD), 1% of this total energy is equivalent to about 3 trillion USD/year. In these bar plots, we can see a clear difference between the results from IGSM-CAM and MIROC, showing that differences in GCM model structure play a major role in the outcome. In fact, comparing *CS3-REF* to *CS3-POL3.7* in 2100, we see that IGSM-CAM projects negative effects from GHG mitigation, while MIROC projects positive effects, although the positive effects projected by MIROC are considerably larger than the negative effects from IGSM-CAM. Since the summer is the most likely season for negative impacts to occur, we show summer changes in

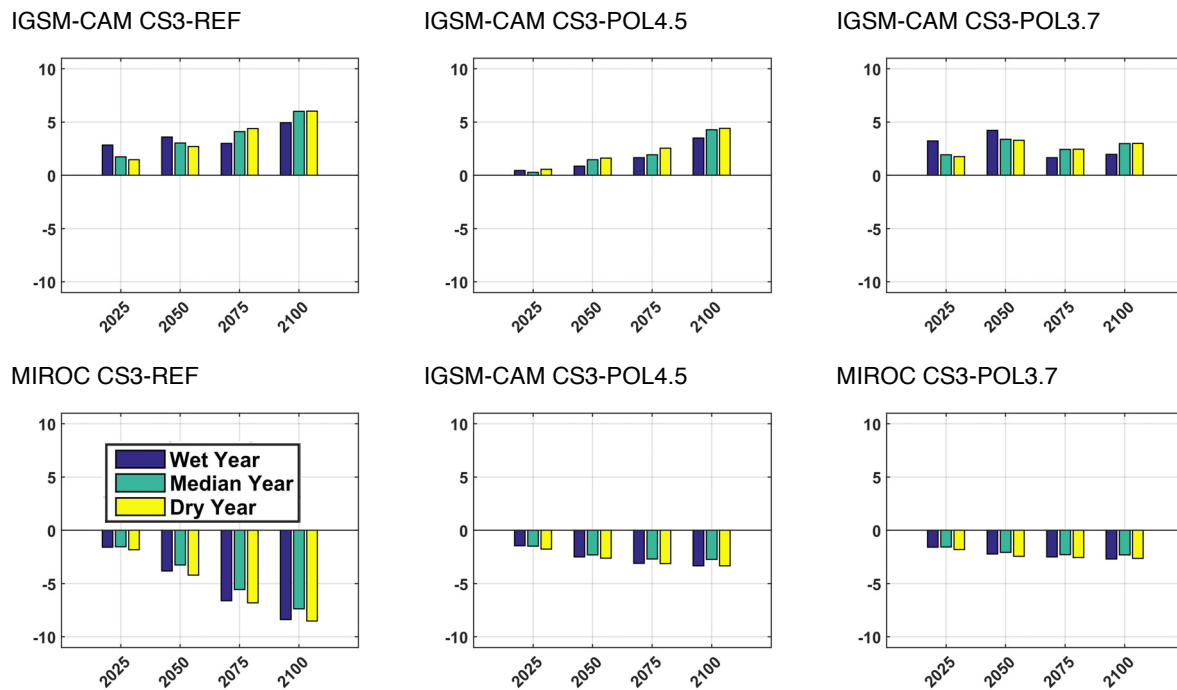


Figure 15. Percent change in total withdrawal allowed weighted by annual generation, where positive is an increase in the allowable withdrawal and negative is a decrease.

allowable withdrawal in **Table 3** for IGSM-CAM and **Table 4** for MIROC. The changes projected by IGSM-CAM for the summer are mild—a result of increased flows and increased temperatures having opposite effects on the allowable withdrawal fraction. For once-through cooling, where we see the largest climate change effect, there is a GHG mitigation benefit of *POL3.7* of about 1.3% in *CS3* and 1.7% in *CS6*, while *CS3-POL4.5* has no benefit. By fuel type, oil benefits the most, although oil accounts for the least annual electricity generation. Coal plants also benefit from *POL3.7* as compared to the reference, with a benefit of 1.2% for both *CS3* and *CS6*. For the MIROC results, allowable withdrawal decreases in the summer for all scenarios and power generation types. Again, once-through cooling benefits the most from *Policy 3.7* mitigation, by 2.3% for *CS3* and 2.9% for *CS6*.

Table 3. IGSM-CAM – Climate change impact on allowable withdrawal in the summer (Jun-Aug) in 2050 for the median-climate year, where positive is an increase in allowable withdrawal and negative is a decrease.

IGSM-CAM		CS3-REF	CS3-pol4.5	CS3-pol3.7	CS6-REF	CS6-pol3.7
Cooling Tech.	Once-Through	-0.8%	-0.9%	2.1%	3.4%	5.1%
	Cooling Tower	0.4%	-0.5%	0.5%	-0.3%	1.5%
	Cooling Pond	0.0%	-0.3%	0.0%	-0.2%	0.0%
Fuel Type	Coal	-0.3%	-0.9%	0.9%	1.1%	2.3%
	Natural Gas	-0.1%	0.0%	0.1%	-0.1%	1.9%
	Nuclear	0.1%	-0.3%	1.0%	1.4%	3.4%
	Other Fossil	-1.3%	-1.1%	1.4%	-4.7%	-2.0%

Table 4. MIROC – Climate change impact on allowable withdrawal in the summer (Jun-Aug) in 2050 for the median-climate year, where positive is an increase in allowable withdrawal and negative is a decrease.

MIROC		CS3-REF	CS3-pol4.5	CS3-pol3.7	CS6-REF	CS6-pol3.7
Cooling Tech.	Once-Through	-6.0%	-4.1%	-3.7%	-8.3%	-5.5%
	Cooling Tower	-1.8%	-1.1%	-1.0%	-2.2%	-1.5%
	Cooling Pond	-0.8%	-0.2%	-0.1%	-0.4%	-0.7%
Fuel Type	Coal	-4.1%	-2.6%	-2.4%	-5.2%	-3.6%
	Natural Gas	-0.7%	-0.4%	-0.4%	-1.0%	-0.5%
	Nuclear	-1.8%	-1.2%	-1.2%	-2.5%	-1.6%
	Other Fossil	-2.5%	-1.8%	-1.1%	-3.1%	-2.1%

4.3 Valuation of Mitigation Benefits

Projections of power prices from ReEDS are used to value the change in thermal generation (see McFarland *et al.*, forthcoming). Scenarios modeling reductions in GHG emissions assume that supply-side costs in the electric sector associated with shifting the generation mix are incorporated into the price of electricity. We consider two illustrative electricity price scenarios that include and exclude the marginal cost of CO₂. Electricity prices inclusive of CO₂ emission costs show higher prices under the mitigation scenarios (e.g., prices in 2050 range from

\$115/MWh in the *REF* scenario to \$127/MWh in the *POL3.7* scenario in 2005\$), whereas excluding emissions costs, prices are relatively similar across scenarios (e.g., 2050 prices are \$115/MWh in *REF* versus \$117/MWh in the *POL3.7* scenario). These two price scenarios produce high- and low-end estimates, respectively, of the benefits of global GHG mitigation on U.S. thermal generation. The high price scenario, inclusive of emission costs, would best reflect the lost value of generation from low-emitting thermal units such nuclear or a fossil technology with carbon capture and storage. The low price scenario, exclusive of emission costs, would reflect the lost value of generation from coal, gas, or oil units without carbon capture. Note that these results do not consider feedbacks between thermal production, prices, and production from other sources—to fully capture the economic effects of changes in thermal power generation potential, we would iterate our model with an electricity sector-planning model such as ReEDS.

Table 5 shows these results for the three emission scenarios under CS values of 3°C and/or 6°C for IGSM-CAM, and **Table 6** shows these results for MIROC. In 2050, under the price scenario including emissions costs, the annual benefits of reducing GHG emissions under the *CS3-POL3.7* scenario are approximately \$35 billion for IGSM-CAM and \$36 billion for MIROC. Excluding emissions costs, the benefits are approximately \$8.3 billion for IGSM-CAM and \$39 million for MIROC. The 2015 to 2050 present value benefits under these two price scenarios for the *POL3.7* scenario, discounted at 3%, are approximately \$536 billion and \$53 billion, respectively, for IGSM-CAM, and \$538 billion and \$65 billion, respectively, for MIROC. The high-end estimate reflects the value of lost generation from no- or low-emitting thermal technologies while the low-end estimate reflects the value of emitting technologies. The actual benefit would reside somewhere in between and depend upon the transition pathway from emitting to non-emitting generation sources.

Table 5. IGSM-CAM – National average change in thermal power revenues (millions of 2005\$) from control in 2025 and 2050 under each of the ReEDS price scenarios.

Price Scenario	Year	CS3-REF	CS3-POL4.5	CS3-POL3.7	CS6-REF	CS6-POL3.7
Emission costs included	2025	\$2,092	\$12,760	\$25,438	\$2,687	\$27,787
	2050	\$3,807	\$15,855	\$38,879	\$7,085	\$42,097
Emission costs excluded	2025	\$2,092	\$2,647	\$3,995	\$2,687	\$6,171
	2050	\$3,807	\$5,532	\$8,268	\$7,085	\$11,210

Table 6. MIROC – National average change in thermal power revenues (millions of 2005\$) from control in 2025 and 2050 under each of the ReEDS price scenarios.

Price Scenario	Year	CS3-REF	CS3-POL4.5	CS3-POL3.7	CS6-REF	CS6-POL3.7
Emission costs included	2025	(\$2,154)	\$9,999	\$21,059	(\$3,035)	\$20,539
	2050	(\$5,888)	\$10,130	\$29,881	(\$8,090)	\$28,095
Emission costs excluded	2025	(\$2,154)	(\$12)	(\$60)	(\$3,035)	(\$542)
	2050	(\$5,888)	(\$17)	\$39	(\$8,090)	(\$1,594)

5. CONCLUSION

We build and validate a standalone river temperature model and apply this generic model to the United States at the 8-digit HUC scale. We demonstrate that the standalone model performs well with a detailed description of flow and geometry. Next, we construct a series of models that represent the system at hand. A rainfall-runoff model is used to convert climate from GCM projections to changes in runoff. In parallel, a water demand model is implemented to develop water demand projections for the various scenarios. Next, a water resource planning model is used to simulate water allocation and management at the HUC-8 scale. The standalone water temperature model is applied to the streamflow and climate output to estimate surface-water temperatures. Finally, we compare regulated withdrawal to demands for withdrawal from thermal power plants in CONUS, and estimate the power generation impact of climate change (represented by changes in allowable withdrawal). We demonstrate that this modeling system performs reasonably well for a generalized 8-digit HUC river for 16 stations of daily water temperature across the United States.

After developing a number of future scenarios with information from two GCMs, two climate sensitivities, and three mitigation policies, we run the system of models for four eras and three climate years: wet, median, and dry. We find that water temperatures increase by 2050 to 1–2°C in the *CS3-REF* case and 0.3–1°C in *CS3-POL3.7*. Temperatures in 2100 do not significantly increase for the stringent GHG mitigation case, *CS3-POL3.7*, while temperatures in *CS3-REF* increase by about 4–6°C annually. Thus, there is a strong incentive to mitigate GHG emissions in order to keep surface water temperatures at reasonable levels. We find that the two GCMs project drastically different patterns of surface water warming—IGSM-CAM projects warming to be more severe in the west, while MIROC projects more warming in the east and the Great Plains. These differences in geographic patterns between the GCMs are partially attributed to the patterns of changes in precipitation, which manifest to changes in streamflow across CONUS—where IGSM-CAM projects substantial increases in streamflow in the majority of the region, and MIROC projects substantial decreases.

These different geographic patterns in climate change projections for the two GCMs result in significant differences in thermal power plant impacts. IGSM-CAM generally projects increases in allowable withdrawal, and the most extreme scenarios—namely, *CS6-REF*—show the greatest benefit to thermal power generation, which rises above 5% annually in 2050. The MIROC projections provide a different picture of the future of thermal power generation, with substantial reductions in potential generation of about 5% at most in 2050, rising to more than 10% in 2100. We then take a more in-depth look into the impacts on the Jun-Aug season. We find that the hotter temperatures in the summer counterbalance most of the increases in runoff from IGSM-CAM, resulting in smaller changes to allowable withdrawal. For MIROC, we find that negative impacts in the summer are also greater, with reductions in allowable withdrawals reaching 6% for *CS3-REF*—much larger than the 0.8% for IGSM-CAM. In spite of the differences, the mitigation benefit of *POL3.7* for the two GCMs is surprisingly close for the summer, at about 1.3% for IGSM-CAM and 2.3% for MIROC.

With the striking differences between the two GCMs used in this analysis, an obvious improvement would be to run the series of models with more GCMs. We believe that these two GCMs represent both a wet climate projection and a dry climate projection, but are not certain if these two GCMs represent extremes in terms of allowable withdrawal or water temperature changes. While adding more GCMs would provide additional points on the uncertainty distribution, we would still only provide the range of points, of which the probabilities are unknown. Another solution would be to analyze this system of models with an ensemble of scenarios similar to Webster *et al.* (2011) and Schlosser *et al.* (2012).

In addition to addressing the issue of climate projection uncertainty, the models used in this analysis also contribute uncertainty in input data, assumptions, and model structure. One way to address this uncertainty is to reduce the spatial or temporal scale of the models. We can also replace or improve the various assumptions—e.g., the assumption of a parabolic river cross-sectional shape for all rivers in CONUS, which might be improved by altering the shape by topography or region. Another potential area of improvement is the detail at which we address power plant withdrawal demand and uptake. We assume a consistent change in the temperature of water released by once-through cooling plants. This heat would likely vary by plant and by capacity factor. Furthermore, water management and power plant facilities are changing over time, both long-term changes (i.e. investments in new facilities and retiring older ones) as well as short-term variations, which respond to changes in food and electricity prices, all of which vary throughout each year, week and day. Future research plans are already in place to address many of these assumptions.

Nevertheless, this study does provide a necessary step to understanding the impacts of climate change on both water temperature and thermal power plant generation.

6. REFERENCES

- Adams, E.E., and R.F. Harleman, 1979: Waste heat management in the electric power industry: issues of energy conservation and station operation under environmental constraints. *Energy Laboratory Report No. MIT-EL 79-040*.
- Allen, R.G., L.S. Pereira, D. Raes, and M. Smith, 1998: Crop evapotranspiration—guidelines for computing crop water requirements. *FAO Irrigation and Drainage*, paper 56.
- Brown, L.C. and T.O. Barnwell, 1987: *The enhanced stream water quality models QUAL2E and QUAL2E-UNCAS: documentation and user manual*. US Environmental Protection Agency, Office of Research and Development, Environmental Research Laboratory.
- Brungs, W.A., B.R. Jones and D.I. Mount, 1977: *Temperature criteria for freshwater fish*. Protocol and Procedures. Environmental Research Laboratory-Duluth. US EPA, Citeseer.
- Chandel, M.K., L.F. Pratson and R.B. Jackson, 2011: The potential impacts of climate-change policy on freshwater use in thermoelectric power generation. *Energy Policy* **39**(10): 6234– 6242.
- Chapra, S.C., 1997: *Surface Water-Quality Modeling*. McGraw-Hill, New York.
- Chapra, S.C., 2008: *Surface water-quality modeling*. Waveland Press. DOE, December 2006: Energy Demands on Water Resources: Report to Congress on the Interdependency of Energy and Water. White Paper.
- Corps [U.S. Army Corps of Engineers], 2013: *National Inventory of Dams*. accessed June 15, 2013 at <http://geo.usace.army.mil/pgis/f?p=397:12>.

- Droogers, P., and R. Allen, 2002: Estimating reference evapotranspiration under inaccurate data conditions. *Irrigation and Drainage Syst.* **16**, 33–45
- EIA [Energy Information Administration], 2013: *Annual Energy Outlook*.
- EPRI [Electric Power Research Institute], 2002: *Water & Sustainability (Volume 3): U.S. Water Consumption for Power Production—The Next Half Century*. EPRI, Palo Alto, CA. 1006786.
- Farmer, W.H. and R.M. Vogel, 2012: Performance-weighted methods for estimating monthly streamflow at ungagged sites. *Journal of Hydrology* **477**, 240-250.
- Förster, H. and J. Lilliestam, 2010: Modeling thermoelectric power generation in view of climate change. *Regional Environmental Change* **10**(4): 327–338.
- Gooseff, M.N., K. Strzpek and S.C. Chapra, 2005: Modeling the potential effects of climate change on water temperature downstream of a shallow reservoir, Lower Madison River, MT. *Climatic Change* **68**(3): 331–353.
- Graham, J., 1949: Some effects of temperature and oxygen pressure on the metabolism and activity of the speckled trout, *Salvelinus fontinalis*. *Canadian Journal of Research* **27**(5): 270–288.
- Gupta V. and S. Sorooshian, 1985: The relationship between data and the precision of parameter estimates of hydrologic models. *J. Hydrol.* **81**, 57–77.
- Herb, W. and H. Stefan, 2010: Projecting the impact of climate change on coldwater stream temperatures in Minnesota using equilibrium temperature models. Project Report.
- IPCC [International Panel on Climate Change], 2014: International Panel on Climate Change 5th Assessment Report.
- Kaczmarek, Z., 1993: Water balance model for climate impact analysis. *ACTA Geophysica Polonica* **41**(4):1–16.
- Kenny, J.F., N.L. Barber, S.H. Susan, K.S. Linsey, J.K. Lovelace and M. Maupin, 2014: Estimated Use of Water in the United States in 2005. United States Geological Survey, *Circular 1344*.
- Kenny, J.F., N.L. Barber, S.S. Hutson, K.S. Linsey, J.K. Lovelace, and M.A. Maupin, 2009: Estimated use of water in the United States in 2005. U.S. Geological Survey *Circular 1344*, 52 p.
- Leopold, L.B. and T. Maddock, 1953: The hydraulic geometry channels and some physiographic implications. Geological Survey *Professional Paper 252*, Washington, D.C.
- MacCormack, R.W., 1969: The effect of viscosity in hypervelocity impact cratering. *Am. Inst. Aeronaut. Astronaut Paper 69*, 354.
- MacLeod, J. and E. Pessah, 1973: Temperature effects on mercury accumulation, toxicity, and metabolic rate in rainbow trout (*Salmo gairdneri*). *Journal of the Fisheries Board of Canada* **30**(4): 485–492.
- Monier, E., J.R. Scott, A.P. Sokolov, C.E. Forest and C.A. Schlosser, 2013: An integrated assessment modeling framework for uncertainty studies in global and regional climate change: the MIT IGSM-CAM (version 1.0). *Geosci. Model Dev.* **6**, 2063–2085, doi: 10.5194/gmd-6-2063-2013.
- Monier, E., X. Gao, J. Scott, A. Sokolov and A. Schlosser, 2014: A framework for modeling uncertainty in regional climate change. *Climatic Change*, doi: 10.1007/s10584-014-1112-5.
- Ngo-Duc, T., T. Oki and S. Kanae, 2007: A variable streamflow velocity method for global river routing model: model description and preliminary results. *Hydrology & Earth System Sciences Discussions* **4**(6).
- Olivera, F., J. Famiglietti and K. Asante, 2000: Global-scale flow routing using a source-to-sink algorithm. *Water Resources Research* **36**(8): 2197–2207.
- Paltsev, S., E. Monier, J. Scott, A. Sokolov and J. Reilly, 2013: Integrated economic and climate projections for impact assessment. *Climatic Change*, doi: 10.1007/s10584-013-0892-3.
- PRISM, 2014: PRISM Climate Group, Oregon State University (<http://www.prism.oregonstate.edu>).

- Sheffield, J., G. Goteti and E.F. Wood, 2006: Development of a 50-year high-resolution global dataset of meteorological forcings for land surface modeling. *J. Climate* **19**: 3088–3111.
- Schlosser, C.A., X. Gao, K. Strzepek, A. Sokolov, C.E. Forest, S. Awadalla and W. Farmer, 2012: Quantifying the likelihood of regional climate change: A hybridized approach. *Journal of Climate* **26**(10): 3394–3414, doi: 10.1175/JCLI-D-11-00730.1.
- Sieber, J., and D. Purkey, 2007: *User Guide for WEAP21*. Stockholm Environment Institute.
- Short, W., P. Sullivan, T. Mai, M. Mowers, C. Uriarte and N. Blair, 2011: Regional Energy Deployment System (ReEDS). Contract, 303, 275–3000.
- Snodgrass, W.J., 1974: *A predictive phosphorus model for lakes: development and testing*. Ph.D. Dissertation, University of North Carolina, Chapel Hill, NC.
- Stefan, H.G. and E.B. Preud'homme, 1993: Stream Temperature Estimation From Air Temperature. *Water Resources Bulletin* **29**(1): 27–45.
- Strzepek, K., A. McCluskey, B. Boehlert, M. Jacobsen and C. Fant, 2011: Climate variability and change: a basin scale indicator approach to understanding the risk to water resources development and management. *Water papers*, Washington, D.C.: World Bank (<http://documents.worldbank.org/curated/en/2011/09/15897484/climate-variability-change-basin-scale-indicator-approach-understanding-risk-water-resources-development-management>).
- Strzepek, K., M. Jacobsen, B. Boehlert and J. Neumann, 2013: Toward evaluating the effect of climate change on investments in the water resources sector: insights from the forecast and analysis of hydrological indicators in developing countries. *Environmental Research Letters* **8**(4):044014.
- UCS [Union of Concerned Scientists], 2012: *UCS EW3 Energy-Water Database V.1.3*. <http://www.ucsusa.org/ew3database>.
- USDA [U.S. Department of Agriculture], 2010: Farm and ranch irrigation survey (2008): Volume 3, Special Studies, Part 1, AC-07-SS-1.
- USFS [U.S. Forest Service], 2014: *Water Supply Stress Index (WaSSI)*. accessed on September 20, 2014 at <http://www.forestthreats.org/research/tools/WaSSI>.
- USWRC [U.S. Water Resources Council], 1978: The Nations' Water Resources 1975-2000. Second National Water Assessment (<http://water.usgs.gov/watercensus/nwr-1975-2000.html>).
- van Vliet, M., J. Yearsley, W. Franssen, F. Ludwig, I. Haddeland, D. Lettenmaier and P. Kabat, 2012a: Coupled daily streamflow and water temperature modelling in large river basins. *Hydrology & Earth System Sciences Discussions* **9**(7).
- van Vliet, M.T., J.R. Yearsley, F. Ludwig, S. Vögele, D.P. Lettenmaier and P. Kabat, 2012b: Vulnerability of US and European electricity supply to climate change. *Nature Climate Change* **2**(9): 676–681.
- Waldhoff, S., J. Martinich, M. Sarofim, B. DeAngelo, J. McFarland, L. Jantarasami, K. Shouse, A. Crimmins and J. Li, 2014: Overview of the special issue: A multi-model framework to achieve consistent evaluation of climate change impacts in the United States. *Climatic Change*, doi: 10.1007/s10584-014-1206-0.
- Walker, J. and J. Lawson, 1993: Natural Stream Temperature Variations in a Catchment. *Water Research* **11**(1): 27–45.
- Webster, M., A.P. Sokolov, J.M. Reilly, C.E. Forest, S. Paltsev, C.A. Schlosser, C. Wang, D. Kicklighter, M. Sarofim, J. Melillo, R.G. Prinn and H.D. Jacoby, 2011: Analysis of climate policy targets under uncertainty. *Climatic Change* **112**(3-4), 569-583.
- Yearsley, J., 2012: A grid-based approach for simulating stream temperature. *Water Resources Research* **48**(3).
- Yearsley, J.R., 2009: A semi-Lagrangian water temperature model for advection-dominated river systems. *Water Resources Research* **45**(12).

REPORT SERIES of the MIT Joint Program on the Science and Policy of Global Change

FOR THE COMPLETE LIST OF JOINT PROGRAM REPORTS: <http://globalchange.mit.edu/pubs/all-reports.php>

241. **Consumption-Based Adjustment of China's Emissions-Intensity Targets: An Analysis of its Potential Economic Effects.** *Springmann et al.*, March 2013
242. **The Energy and CO₂ Emissions Impact of Renewable Energy Development in China.** *Zhang et al.*, April 2013
243. **Integrated Economic and Climate Projections for Impact Assessment.** *Paltsev et al.*, May 2013
244. **A Framework for Modeling Uncertainty in Regional Climate Change.** *Monier et al.*, May 2013
245. **Climate Change Impacts on Extreme Events in the United States: An Uncertainty Analysis.** *Monier and Gao*, May 2013
246. **Probabilistic Projections of 21st Century Climate Change over Northern Eurasia.** *Monier et al.*, July 2013
247. **What GHG Concentration Targets are Reachable in this Century?** *Paltsev et al.*, July 2013
248. **The Energy and Economic Impacts of Expanding International Emissions Trading.** *Qi et al.*, August 2013
249. **Limited Sectoral Trading between the EU ETS and China.** *Gavard et al.*, August 2013
250. **The Association of Large-Scale Climate Variability and Teleconnections on Wind Resource over Europe and its Intermittency.** *Kriesche and Schlosser*, September 2013
251. **Regulatory Control of Vehicle and Power Plant Emissions: How Effective and at What Cost?** *Paltsev et al.*, October 2013
252. **Synergy between Pollution and Carbon Emissions Control: Comparing China and the U.S.** *Nam et al.*, October 2013
253. **An Analogue Approach to Identify Extreme Precipitation Events: Evaluation and Application to CMIP5 Climate Models in the United States.** *Gao et al.* November 2013
254. **The Future of Global Water Stress: An Integrated Assessment.** *Schlosser et al.*, January 2014
255. **The Mercury Game: Evaluating a Negotiation Simulation that Teaches Students about Science-Policy Interactions.** *Stokes and Selin*, January 2014
256. **The Potential Wind Power Resource in Australia: A New Perspective.** *Hallgren et al.*, February 2014
257. **Equity and Emissions Trading in China.** *Zhang et al.*, February 2014
258. **Characterization of the Wind Power Resource in Europe and its Intermittency.** *Cosseron et al.*, March 2014
259. **A Self-Consistent Method to Assess Air Quality Co-Benefits from US Climate Policies.** *Saari et al.*, April 2014
260. **Electricity Generation and Emissions Reduction Decisions under Policy Uncertainty: A General Equilibrium Analysis.** *Morris et al.*, April 2014
261. **An Integrated Assessment of China's Wind Energy Potential.** *Zhang et al.*, April 2014
262. **The China-in-Global Energy Model.** *Qi et al.* May 2014
263. **Markets versus Regulation: The Efficiency and Distributional Impacts of U.S. Climate Policy Proposals.** *Rausch and Karplus*, May 2014
264. **Expectations for a New Climate Agreement.** *Jacoby and Chen*, August 2014
265. **Coupling the High Complexity Land Surface Model ACASA to the Mesoscale Model WRF.** *Xu et al.*, August 2014
266. **The CO₂ Content of Consumption Across US Regions: A Multi-Regional Input-Output (MRIO) Approach.** *Caron et al.*, August 2014
267. **Carbon emissions in China: How far can new efforts bend the curve?** *Zhang et al.*, October 2014
268. **Characterization of the Solar Power Resource in Europe and Assessing Benefits of Co-Location with Wind Power Installations.** *Bozonnat and Schlosser*, October 2014
269. **A Framework for Analysis of the Uncertainty of Socioeconomic Growth and Climate Change on the Risk of Water Stress: a Case Study in Asia.** *Fant et al.*, November 2014
270. **Interprovincial Migration and the Stringency of Energy Policy in China.** *Luo et al.*, November 2014
271. **International Trade in Natural Gas: Golden Age of LNG?** *Du and Paltsev*, November 2014
272. **Advanced Technologies in Energy-Economy Models for Climate Change Assessment.** *Morris et al.*, December 2014
273. **The Contribution of Biomass to Emissions Mitigation under a Global Climate Policy.** *Winchester and Reilly*, January 2015
274. **Modeling regional transportation demand in China and the impacts of a national carbon constraint.** *Kishimoto et al.*, January 2015.
275. **The Impact of Advanced Biofuels on Aviation Emissions and Operations in the U.S.** *Winchester et al.*, February 2015
276. **Specifying Parameters in Computable General Equilibrium Models using Optimal Fingerprint Detection Methods.** *Koesler*, February 2015
277. **Renewables Intermittency: Operational Limits and Implications for Long-Term Energy System Models.** *Delarue and Morris*, March 2015
278. **The MIT EPPA6 Model: Economic Growth, Energy Use, and Food Consumption.** *Chen et al.*, March 2015
279. **Emulating maize yields from global gridded crop models using statistical estimates.** *Blanc and Sultan*, March 2015
280. **Water Body Temperature Model for Assessing Climate Change Impacts on Thermal Cooling.** *Strzepek et al.*, May 2015